RESEARCH Open Access



NSH76: a selective inhibitor of RRN3 and RNA polymerase I transcription with potential for cancer therapy

Shashanka Shekhar Sarkar¹, Mansi Sharma¹, Arpita Karmakar¹, Kousar Jahan², Sheetanshu Saproo¹, Soumojit Biswas³, Sakshi Nautiyal³, Ipsita Roy³, P. V. Bharatam² and Srivatsava Naidu^{1*}

Abstract

Background Aberrant upregulation of RNA polymerase I (Pol I) transcription and its dedicated machinery plays a pivotal role in tumor progression and chemoresistance. RRN3, a Pol I-specific transcription initiation factor, is frequently overexpressed in malignancies contributing to oncogenic processes. Despite the therapeutic potential of Pol I transcription inhibition, existing inhibitors lack specificity and are associated with DNA damage, mutagenicity, and toxicity, limiting their clinical utility. To fully realize the potential of Pol I-targeted cancer therapies, selective Pol I transcription inhibitors with minimal off-target effects are essential.

Methods Molecular docking and virtual screening were conducted to identify ligands targeting RRN3. Biochemical and spectroscopic analyses validated the direct ligand-RRN3 binding. The mechanism of action of the ligand was investigated through biochemical, cellular and molecular assays. Functional studies assessed the effects of the ligand on cancer cell viability, clonogenicity, cell cycle progression, and apoptosis, in comparison to non-cancerous cells. The ligand efficacy was further evaluated in chemoresistant cancer cell lines and 3D tumor spheroid models. Genotoxicity and mutagenicity were assessed using DNA damage and mutagenicity assays.

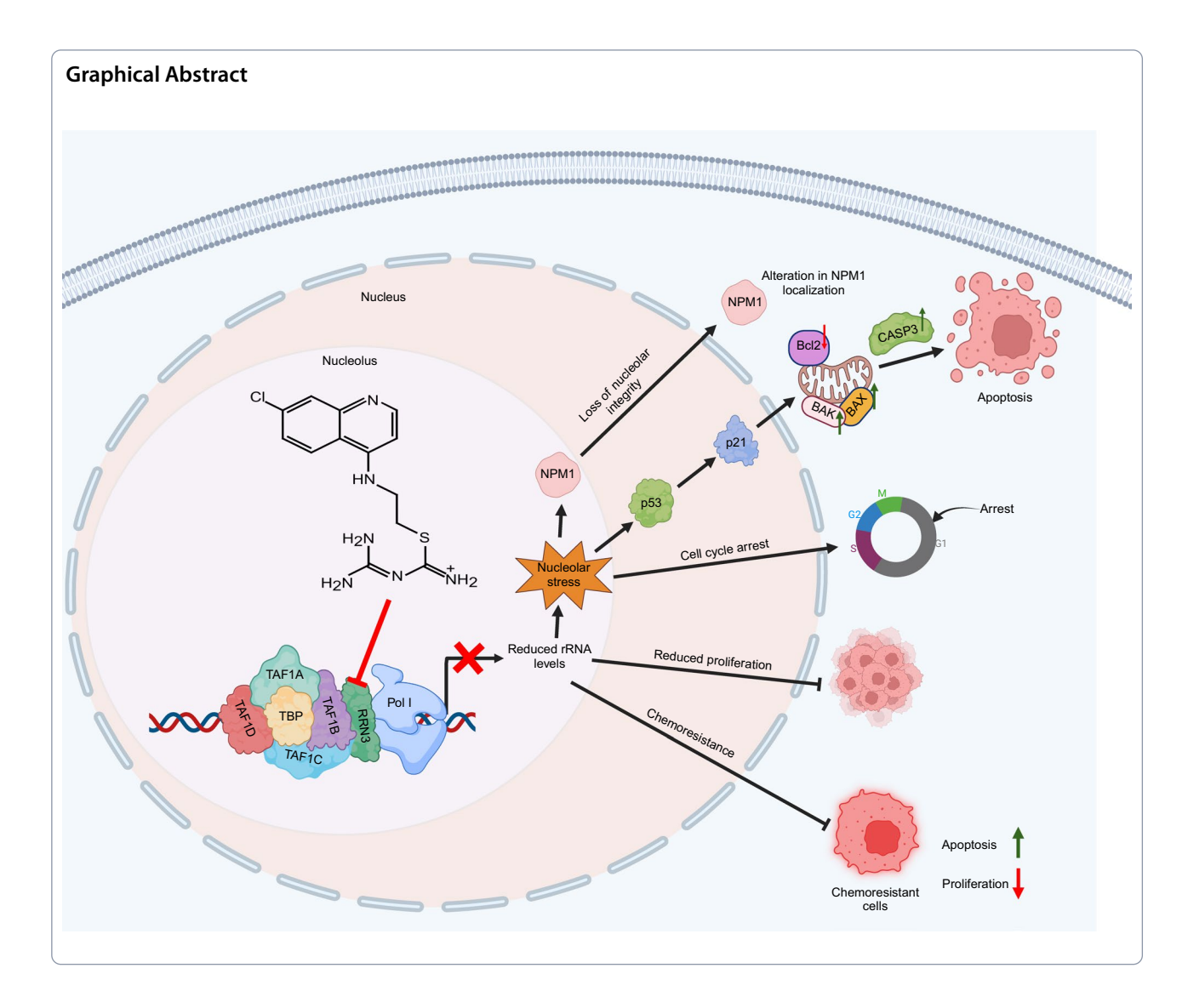
Results We demonstrate that (N-(1-amidino-2-thiourea-alkyl-7-chloroquinoline-4-amine)) (NSH76) selectively inhibits Pol I transcription by disrupting the Pol I pre-initiation complex at the rDNA promoter through direct RRN3 binding. Notably, NSH76 does not affect cMyc expression, a Pol II-driven transcript, confirming its specificity. NSH76 preferentially inhibits Pol I transcription in cancer cells with high RRN3 expression, while sparing non-cancerous cells with low RRN3 levels. Functionally, NSH76 exhibits potent antiproliferative activity against cancer cells, with minimal impact on non-cancerous cells. NSH76 induces cell cycle arrest, suppresses clonogenicity, and significantly enhances apoptosis in cancer cells, including cisplatin- and doxorubicin-resistant cell lines. These effects are recapitulated in 3D tumor spheroid assays. Furthermore, NSH76 triggers nucleolar stress, leading to the activation of tumor suppressors p53 and p21. Notably, NSH76 does not induce DNA damage or mutagenicity.

Conclusion These findings establish NSH76 as a potent and selective Pol I inhibitor with significant therapeutic potential in cancer and possible implications for overcoming chemoresistance.

Keywords RNA polymerase I transcription, Cancer therapy, Selective inhibition, Chemoresistance, RRN3, Antineoplastic compounds, Genotoxicity, Targeting basal transcriptional machinery

*Correspondence: Srivatsava Naidu srivatsava.naidu@iitrpr.ac.in Full list of author information is available at the end of the article





Introduction

RNA Polymerase I (Pol I) transcription synthesizes ribosomal RNA (rRNA), a critical component of ribosome biogenesis and function [1]. The transcriptional output of Pol I directly regulates cellular growth, proliferation, differentiation, and survival by modulating ribosomal abundance and protein synthesis capacity [2, 3]. In cancer, Pol I transcription is frequently dysregulated, and its hyperactivity is considered as a hallmark of malignancy. However, its extent and impact vary by cancer subtype, largely due to genetic alterations and oncogenic signals that upregulate Pol I machinery and rDNA transcription [4]. Elevated expression of Pol I transcriptional machinery drives oncogenic phenotypes, contributes to poor prognosis, and promotes resistance to therapies [5-10]. Furthermore, aberrant rRNA modifications can alter translational fidelity and efficiency, further accelerating tumor cell proliferation and survival [11]. Collectively, these findings underscore the pivotal role of hyperactive Pol I transcription in cancer pathogenesis and highlight its potential as a target for therapy.

The initiation of Pol I transcription requires the assembly of a pre-initiation complex (PIC) at the ribosomal DNA (rDNA) promoter, comprising Pol I-specific components: Selectivity Factor 1 (SL1), Upstream Binding Factor (UBF), RRN3, and Pol I. SL1, a complex of TATA-binding protein (TBP) and TBP-associated factors (TAFs: TAF1 A, TAF1B, TAF1 C, and TAF1D), recognizes the core promoter and stabilizes UBF binding to the upstream control element. RRN3 interacts with SL1/UBF, and is critical for Pol I recruitment to the transcription start site [2, 12]. These protein–protein and protein-rDNA interactions not only initiate Pol I transcription but also serve as regulatory hubs for fine-tuning rRNA synthesis. Oncogenes such as cMyc, RAS, PI3 K, and nucleophosmin stimulate PIC assembly, while tumor

suppressors pRB, p53, and PTEN exert inhibitory effects [13]. Disruption of this regulatory balance during carcinogenesis leads to hyperactive rRNA synthesis, fueling uncontrolled cancer cell proliferation, and other associated malignant features [6]. Notably, increased expression of PIC components, including SL1, RRN3, UBF, and Pol I core subunits, has been observed across multiple cancer types [14–18]. Genetic inhibition of these components has demonstrated anti-tumor effects in vitro and in vivo [15–17], underscoring their potential as druggable targets for cancer therapy.

Elevated rRNA synthesis is a hallmark of cancer cells, whereas normal cells maintain relatively low levels. This disparity makes cancer cells more vulnerable to inhibition of rRNA production, providing a strong rationale for Pol I-targeted therapies [13, 19]. CX-5461 [20] and BMH-21 [21, 22] have been proposed as selective inhibitors of Pol I transcription that have shown promise in preclinical models. However, their clinical utility is limited by significant off-target effects. CX-5461, designed to selectively inhibit Pol I, primarily targets topoisomerase IIB (TOP2B), with TOP2B levels determining CX-5461 sensitivity in cancer cells [23], and also induces DNA damage [24]. Similarly, BMH-21 exhibits off-target effects, including non-specific degradation of Pol II, TOP2B inhibition, and cause DNA damage [25]. These limitations underscore the need for novel, more specific therapeutics to fully exploit Pol I transcriptional inhibition for cancer treatment.

RRN3, an essential component of the PIC, functions as a critical regulatory checkpoint for rRNA synthesis [26]. Emerging evidence underscores the oncogenic role of RRN3 in cancer. Genetic silencing of RRN3 in breast cancer cells significantly reduced rRNA transcription and suppressed cell proliferation, that was rescued upon RRN3 overexpression [15]. Similarly, in pancreatic cancer xenograft models, genetic inhibition of RRN3 markedly decreased tumor burden [14]. In lung adenocarcinoma (LUAD), microRNA-mediated suppression of RRN3 demonstrated potent anti-tumor activity both in vitro and in vivo [16]. Together, these findings establish RRN3 as a promising molecular target for therapeutic inhibition of Pol I transcription.

Here, we identified (N-(1-amidino-2-thiourea-alkyl-7-chloroquinoline-4-amine)), previously characterized for its antimalarial activity [27], herein referred to as NSH76, as a selective and potent inhibitor of RRN3. NSH76 specifically disrupts rRNA synthesis by inhibiting RRN3-dependent PIC assembly at the rDNA promoter, without affecting Pol II transcription. This targeted inhibition preferentially suppresses cancer cell proliferation over non-cancerous cells, disrupts cell cycle progression, and enhances apoptosis, including activation of the p53

pathway. Notably, NSH76 induces substantial apoptosis in cisplatin- and doxorubicin-resistant cells without causing DNA damage or mutagenesis. Collectively, these findings establish NSH76 as a potent, non-genotoxic inhibitor of Pol I transcription with significant therapeutic potential for targeted cancer therapy.

Materials and methods

Details of all the primers and antibodies used in this study are listed in Additional file 1: Table 1

Computational analyses

The gene expression levels of RRN3 in cancer were analyzed using RNA sequencing data obtained from The Cancer Genome Atlas(TCGA) via OncoDB [28]. Receiver operating characteristic (ROC) curves for LUAD, Prostate adenocarcinoma (PRAD), and Breast cancer (BRCA) were generated using the ROC plotter tool [29]. Singlecell RNA sequencing data for LUAD, PRAD, and BRCA were retrieved from the 10X Genomics database and analyzed using the Loupe Browser. Differential expression of RRN3 was visualized across K-means clustering (K = 6) for LUAD, PRAD, and BRCA. Gene Set Enrichment Analysis (GSEA) was performed using iDEP.96 (http://bioinformatics.sdstate.edu/idep96/), and results were visualized as an alluvial plot using SRplot (https://www.bioinformatics.com.cn/srplot).

Molecular docking and simulation of RRN3-NSH76 interaction

The cryo-EM structure of human RRN3 was retrieved from the RCSB Protein Data Bank (PDB ID: 7OBA, [30]). The structure was pre-processed to minimize structural anomalies using the Protein Preparation Wizard tool within the Schrödinger suite. Molecular docking was performed using the Schrödinger Glide module, with in-house ligand libraries screened against the prepared RRN3 structure. The stability of the resulting protein-ligand complexes was assessed through 100-ns molecular dynamics simulations using the Desmond software (www.schrodinger.com/citations/). Trajectory analysis was conducted to calculate root mean square deviation (RMSD) values and to determine protein-ligand interaction frequencies over the simulation period.

NSH76 synthesis

NSH76 was synthesized as previously described [27]. Briefly, 4,7-dichloroquinoline (1 mmol) was reacted with ethanolamine (1 mL) at 130 °C for 3 h, followed by precipitation with cold water to yield a white solid intermediate (2) with a yield of 95–98%. This intermediate was then treated with hydrobromic acid and sulfuric acid under cold conditions, refluxed at 140 °C for 6 h, and extracted with dichloromethane (DCM) at pH 7 to obtain

compound (3) with a yield of 85–95%. Finally, compound 3 was refluxed with acetonitrile (ACN) for 12–24 h and purified through successive washes with DCM, MeCN, and ethyl acetate, yielding NSH76 with an 82% yield.

Cell culture

Human cancer cell lines—A549 (LUAD), PC3 (prostate cancer), LNCaP (prostate cancer), and MCF7 (breast cancer)—and non-cancerous cell lines—BEAS-2B (bronchial epithelial), RWPE-1 (prostate), and MCF10 A (mammary)—along with Chinese hamster lung fibroblast V79 cells, were obtained from the National Center for Cell Science (NCCS, Pune, India). Cells were cultured in media as follows: RPMI 1640 for A549, LNCaP, and RWPE-1; Ham's F-10 for PC3; and DMEM for MCF7, V79, and BEAS-2B (all media from Gibco, Thermo Fisher Scientific, USA). Media were supplemented with 10% heat-inactivated fetal bovine serum (Gibco) and 1% penicillin—streptomycin (Gibco). Cells were maintained at 37 °C in a humidified incubator with 5% CO₂.

Tumor spheroid preparation

Tumor spheroids were generated using a previously established protocol [31]. Briefly, 1×10^4 cells (A549, PC3, or MCF7) were seeded into agarose-coated 96-well plates and incubated at 37 °C in a 5% CO $_2$ atmosphere. Spheroids with diameters exceeding 500 μm were selected for subsequent experiments.

Generation of drug-resistant cells

Cisplatin- and doxorubicin-resistant A549 cell lines were established using a dose escalation protocol, as previously described [32]. In brief, A549 cells were initially exposed to 1 μM cisplatin and 0.2 μM doxorubicin for 48 h. Over a period of 6 months, drug concentrations were gradually increased to 10 μM cisplatin and 1 μM doxorubicin. The development of resistance was assessed by comparing the viability and apoptosis levels of resistant cells to those of parental A549 cells following drug treatments.

Drug treatments

In all experiments, cells or spheroids were treated with NSH76 at its half-maximal inhibitory concentration (IC-50). Cisplatin (A549-Cis $^{\rm R}$) and doxorubicin (A549-Dox $^{\rm R}$) resistant A549 cell lines, and control A549 cells were treated with cisplatin (Sigma-Aldrich) at concentrations of 5, 10, and 15 μM or doxorubicin (Sigma-Aldrich) at concentrations of 0.5, 1, and 1.5 μM , respectively. The control group received dimethyl sulfoxide (DMSO) as a vehicle.

Immunoblotting

50 μg of total protein was separated using 8%, 10%, or 12% SDS-PAGE gels (Bio-Rad), and subsequently transferred onto PVDF membranes (Bio-Rad). Membranes were then incubated with the appropriate primary antibodies (detailed in Additional file 1: Table 1). Detection of protein bands was achieved using the Novex[®] ECL chemiluminescent substrate (Thermo Fisher Scientific), and signals were captured using the ChemiDoc Imaging System (Bio-Rad). Band intensities were quantified using Image Lab software (Bio-Rad).

RRN3 protein expression and purification

The open reading frame of RRN3 was cloned into the pET28b-His6 vector (Novagen, Cat #69865-3) using NdeI and NheI restriction sites. Positive clones were verified by PCR and restriction digestion. Escherichia coli BL21 (DE3) cells were transformed with pET28b-His6-RRN3, and a single colony was cultured at 37 °C with shaking (200 rpm) until the optical density at 600 nm (OD600) reached 0.6-0.8. Protein expression was induced with 1 mM isopropyl β-D-1-thiogalactopyranoside at 20 °C for 8 h. The protein was purified by immobilized metal ion affinity chromatography using a Ni2+-NTA matrix and eluted with a buffer containing 20 mM HEPES and 200 mM imidazole at 4 °C for 2 h. Protein concentration was determined using the Bradford protein assay kit (Bio-Rad Laboratories, Hercules, CA, USA). Purification was monitored by 12% sodium dodecyl sulfate-polyacrylamide gel electrophoresis (SDS-PAGE), and protein identity was confirmed by immunoblotting.

RRN3-NSH76 affinity study

The interaction between RRN3 and NSH76 was analyzed using the Drug Affinity Responsive Target Stability (DARTS) assay [33] with minor modifications. Briefly, A549 cells (1×10^6) were cultured to 70–75% confluency, washed with phosphate-buffered saline (PBS), and lysed in cell lysis buffer (150 mM NaCl, 30 mM Tris Base, 0.1% Triton X-100, and 10% glycerol) supplemented with a protease inhibitor cocktail (Roche). Protein concentration was quantified using the Bradford protein assay kit after the addition of 1x TNC buffer (Tris, NaCl, and CaCl₂). The protein lysate was incubated with 50–200 µM NSH76 or DMSO (control) for 1 h at 37 °C. Following incubation, the ligand-bound protein lysate was subjected to proteolysis with Pronase (1:4800 ratio) for 30 min at 37 °C. The reaction was terminated by adding LDS-PAGE loading buffer, and proteins were resolved on an 8% PAGE gel. Proteins were transferred to a polyvinylidene difluoride (PVDF) membrane, probed for RRN3

and GAPDH, and detected using an enhanced chemiluminescence (ECL) substrate on the ChemiDoc imaging system (Bio-Rad).

Circular dichroism spectroscopy of RRN3-NSH76 complex

Circular dichroism (CD) spectroscopy was employed to investigate the structural properties of the RRN3-NSH76 complex. CD measurements were performed on a JASCO J-815 Spectropolarimeter (Jasco International Co. Ltd., Japan). Recombinant RRN3 protein was dialyzed into 20 mM Tris–HCl (pH 7.8) and quantified using the Bradford protein assay kit. CD spectra were recorded for RRN3 protein solutions (6.5 μ M) in 20 mM Tris–HCl (pH 7.8) at 25 °C. Spectral data were collected across a wavelength range of 200–300 nm, with a step size of 2 nm and a dwell time of 4 s per measurement. All spectra were baseline-corrected against the corresponding buffer blank.

RNA isolation and real-time quantitative PCR

To investigate the effects of NSH76 on gene expression, A549, PC3, and MCF7 cells were treated with NSH76 for 15 min, 30 min, 1 h, 2 h, 4 h, or 24 h. Total RNA was isolated from the cells using TRIzol reagent (Ambion, Thermo Fisher Scientific, Waltham, MA, USA) according to the manufacturer's instructions. For quantitative gene expression analysis, 1000 ng of total RNA was reverse-transcribed into cDNA using the PrimeScript[™] 1st strand cDNA Synthesis Kit (TaKaRa Biotechnology Co., Ltd.). Real-time quantitative PCR (qPCR) was performed using TB Green® Premix Ex Tag[™] (Tli RNaseH Plus) (TaKaRa Biotechnology, Japan). Gamma-actin was used as an internal control to normalize gene expression. The primer sequences used are listed in Additional File 1: Table 1. Relative gene expression was calculated using the $2^{-\Delta \Delta Ct}$ method [34].

5-Ethynyl uridine incorporation assay

To assess nascent RNA synthesis, cells were treated with NSH76, BMH-21, or DMSO for 24 h. Subsequently, cells were pulsed with 100 μM 5-ethynyl-2 $^{\prime}$ -uridine (EU) (Sigma-Aldrich) for 1 h at 37 $^{\circ}$ C in a humidified atmosphere containing 5% CO2. EU incorporation was detected using a click chemistry-based assay. Cells were stained with 15 μM azide-fluor (Sigma-Aldrich) for 30 min, followed by counterstaining with Hoechst 33342 (Invitrogen) for 5 min. Nascent RNA synthesis was visualized using a Leica DMi8 fluorescence microscope (Leica Imaging Systems, Germany).

Immunofluorescence

A549, PC3, MCF7, and V79 cells (1×10^5) were seeded on coverslips in 6-well plates and treated with NSH76 (IC-50 concentration) or vehicle control. Alternatively, isolated

spheroids were treated with NSH76 IC-50 concentration. Both cell monolayers and spheroids were fixed with 3.7% formaldehyde for 10 min, permeabilized with 0.1% Triton X-100, and blocked with 5% bovine serum albumin (BSA) for 1 h. Samples were then incubated overnight with primary antibody, followed by a 45-min incubation with secondary antibody. Nuclei were counterstained with Hoechst 33342 (Invitrogen). Coverslips were mounted using Dibutyl phthalate Polystyrene Xylene (DPX) and imaged using a Leica DMi8 fluorescence microscope.

Chromatin-immunoprecipitation assay

ChIP was performed as previously described [16]. A549 cells (1×10^6) were seeded in 10-cm dishes and incubated for 24 h. Cells were then treated with NSH76 or DMSO for 24 h, followed by cross-linking with 1% formaldehyde (Sigma-Aldrich) for 10 min at room temperature (RT). Cross-linking was quenched with 0.125 M glycine (Himedia) for 5 min at RT. Cells were lysed and sonicated using a SinapTec Lab 120 (France) to generate 200-500 bp DNA fragments. For immunoprecipitation, Protein A magnetic beads (BioBharati Life Sciences, India) were pre-incubated with IgG, RRN3, TAF1B, or POLR1B antibodies for 3 h at RT. Sonicated chromatin was then added to antibody-bound beads and incubated for 2 h at RT. Bead-bound DNA-protein complexes were isolated using an extraction buffer, treated with RNase and Proteinase K, and eluted using a QIAGEN PCR purification kit. The relative enrichment of RRN3, TAF1B, and POLR1B on the rDNA promoter was quantified by qPCR.

Cell viability assay

Cells were seeded at a density of 3×10^3 cells/well in 96-well plates and incubated for 24 h. Cells were then treated with NSH76 at concentrations of 2.5, 5, or 10 μ M (cancerous cells) or 10, 20, or 40 μ M (non-cancerous cells) for 24 h. Resistant cells were treated with NSH76, cisplatin, doxorubicin, or DMSO for 24 h. Cell viability was assessed using the Alamar Blue Cell Viability Reagent (Invitrogen) according to the manufacturer's instructions. Absorbance was measured at 570 nm using a CLARIOstar plate reader (BMG Labtech, Ortenberg, Germany).

Carboxyfluorescein succinimidyl ester cell proliferation assav

Cell proliferation was assessed using the CFSE assay. A549, PC3, or MCF7 cells (1.5×10^5) were seeded in 6-well plates overnight. Cells were then treated with NSH76 or DMSO for 24 h, harvested by trypsinization, and washed with ice-cold Dulbecco's phosphate-buffered saline (DPBS). Cells were labelled with 1 μ M CFSE dye

(Invitrogen) at 37 °C for 20 min, followed by washing with DPBS to remove excess dye. CFSE fluorescence was analysed using a BD Accuri[™] C6 Plus Flow Cytometer (BD Biosciences). Data were processed using FlowJo software (BD Biosciences).

Colony formation assay

A549, PC3, or MCF7 cells (1×10^3) were seeded in a sixwell plate and incubated for 24 h. Cells were then treated with NSH76 or DMSO for 24 h. After treatment, cells were washed with DPBS, and complete media was added. The experiment continued until isolated colonies formed. Colonies were then washed with DPBS, fixed with icecold absolute methanol for 5 min, stained with 0.01% (w/v) crystal violet (Sigma-Aldrich) for 20 min at RT, and counted using ImageJ software.

Cell cycle analysis

A549, PC3, or MCF7 cells (1.5×10^5) were seeded in 6-well plates and incubated overnight. Cells were then treated with NSH76 or DMSO for 24 h, harvested by trypsinization, and washed with DPBS. Cells were fixed in 70% ethanol for 2 h at 4 °C, washed, and stained with Propidium Iodide (PI) using the PI Flow Cytometry Kit (Abcam) according to the manufacturer's instructions. Cell cycle distribution was analyzed using a BD AccuriTM C6 Plus Flow Cytometer, and data were processed using FlowJo software.

Apoptosis assay

Apoptosis was evaluated using the Annexin-V-PI Apoptosis Detection Kit I (BD Pharmingen). A549, PC3, MCF7, BEAS-2B, RWPE-1, MCF10 A, A549-Cis^R, or A549-Dox^R cells (1.5×10^5) were treated with NSH76, cisplatin, or doxorubicin for 24 h. Cells were then harvested by trypsinization, washed with DPBS, and stained with Annexin V and PI according to the manufacturer's protocol. Apoptotic cells were analyzed using a BD AccuriTM C6 Plus Flow Cytometer, and data were processed using FlowJo software.

Wound healing assay

A total of 1.5×10^5 A549, PC3, and MCF7 cells were seeded in 6-well plates and allowed to adhere for 18 h. Cells were then treated with the respective IC₅₀ concentrations of NSH76. After 24 h of treatment, a scratch was introduced in the confluent monolayer using a sterile pipette tip. Wound closure was monitored and imaged at 0-, 24-, 48-, and 72-h post-scratch using an EVOS XL light microscope.

Matrigel invasion assay

Matrigel (diluted 1:5 with serum-free media) was added to the top chamber of a 6-well transwell plate (500 $\mu L/$ well). Complete media was added to the bottom chamber. A total of 1×10^5 cells per well (A549, PC3, or MCF7) were seeded in the top chamber. After 24 h of NSH76 treatment at their respective IC50 concentrations, cells were fixed with ice-cold methanol for 10 min. The cells were then stained with 0.01% crystal violet for 10 min and washed twice with DPBS for 5 min each. Non-migrated cells were gently removed using a sterile cotton bud. Migrated cells were imaged using an EVOS XL light microscope.

Alkaline comet assay

The alkaline comet assay was performed according to a previously published protocol [35] with minor modifications. A549 cells (1.5×10^5) were treated with NSH76, doxorubicin, or DMSO for 24 h. Cells were then embedded in 1% low-melting agarose on glass slides. Following overnight lysis at 4 °C, slides were incubated in alkaline electrophoresis solution (pH > 13) for 30 min, followed by electrophoresis at 15 V for 30 min. Slides were then washed with distilled water and ethanol, stained with 20 µg/mL ethidium bromide, and dried at 37 °C. Comet images were captured using a Leica DMi8 fluorescence microscope.

Mutagenesis assay

The mutagenesis assay was performed as previously [36]. Briefly, V79 cells (1.5×10^5) were seeded in 12-well plates and exposed to NSH76, benzopyrene (Sigma-Aldrich), or DMSO for 24 h. Following treatment, 500 cells were reseeded to allow for phenotype expression and incubated for 7 days. Cells were then seeded at a density of 1×10^5 cells/well and selectively cultured in medium containing 6-thioguanine (Sigma-Aldrich) for 9 days. Surviving colonies were stained with crystal violet and counted to assess mutagenic potential.

Micronucleus assay

V79 cells (1.5×10^5) were seeded onto glass coverslips and cultured overnight. The following day, cells were treated with NSH76, etoposide (Sigma-Aldrich), or DMSO for 24 h. After treatment, cells were fixed with ice-cold methanol for 10 min, stained with 1 µg/mL Hoechst-33342 (Invitrogen), and mounted as permanent slides using a mounting medium. Micronuclei were visualized and imaged using a Leica DMi8 fluorescence microscope.

Statistics

All experiments were performed in at least in biological triplicates. Data are presented as mean ± standard error of the mean (SEM) and were analysed using GraphPad Prism software (version 8.2). Statistical significance was determined using two-tailed Student's t-tests for pairwise comparisons or one-way analysis of variance (ANOVA) with Tukey's post-hoc test for multiple group

comparisons. A p-value of \leq 0.05 was considered statistically significant.

Results

Elevated RRN3 expression positively correlates with cancer hallmarks and poor therapeutic response

Given that Pol I transcription is upregulated in LUAD [16], PRAD [37], and BRCA [15], we analyzed RNA-Seq data from TCGA to assess RRN3 expression. Our analysis

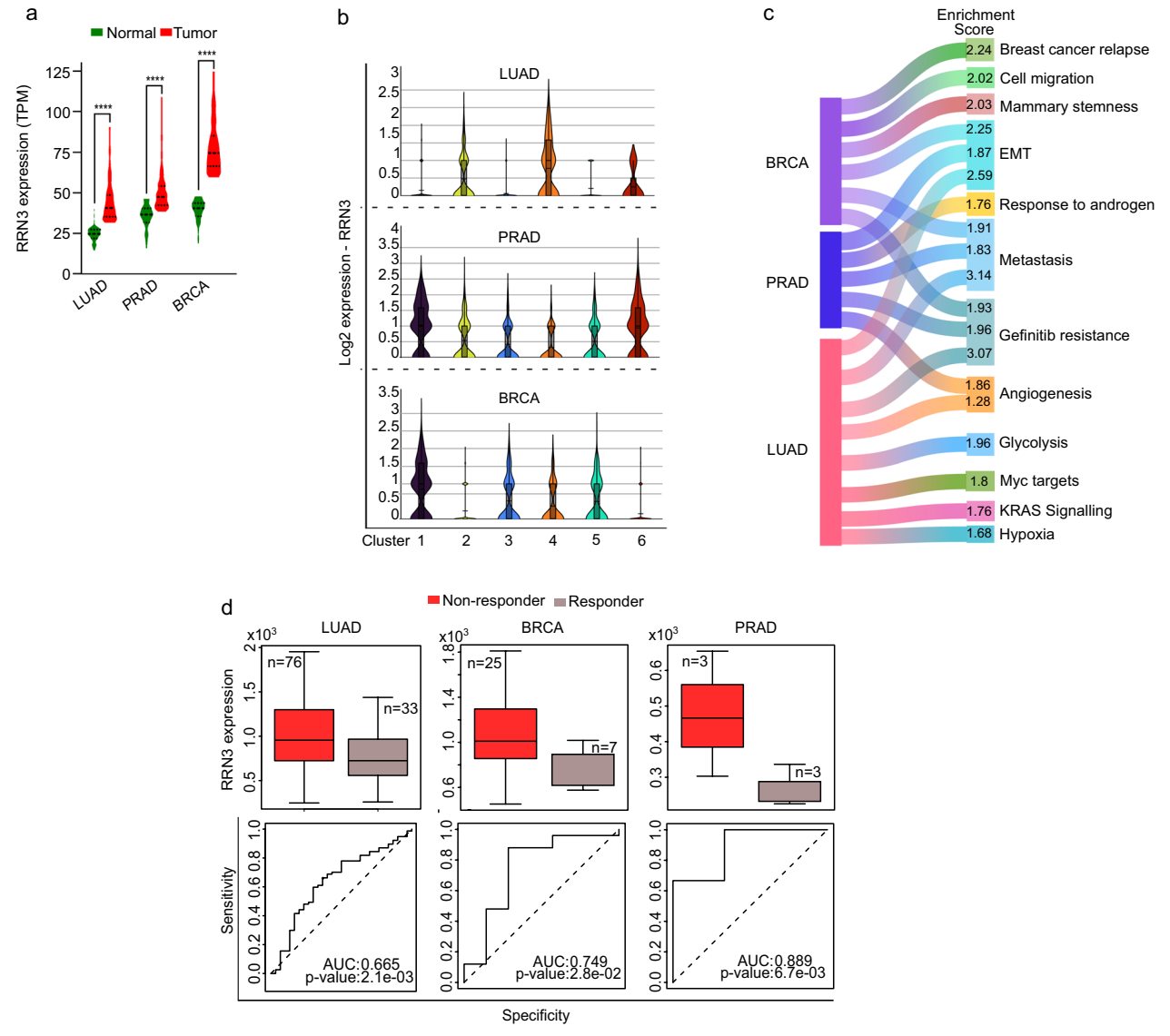


Fig. 1 Elevated RRN3 expression is associated with cancer hallmarks. **a** Violin plot showing upregulation of RRN3 expression in Lung adenocarcinoma (LUAD), Prostate adenocarcinoma (PRAD), Breast cancer (BRCA), compared to normal controls. **b** Unsupervised clustering of single cell RNA-sequencing data showing a distinct RRN3-high cellular subset in BRCA, PRAD, and LUAD. **c** Gene set enrichment analysis (GSEA) of RRN3-high cells in BRCA, PRAD, and LUAD reveals significant enrichment of genes associated with various hallmarks of cancer. **d** Box plots illustrating higher RRN3 expression in patients not responding to therapy compared to responders in LUAD, BRCA, and PRAD (*upper panel*). Receiver Operating Characteristic curves depicting the area under the curve (AUC > 0.5, significant) values for RRN3 expression in predicting drug response in LUAD, BRCA, and PRAD (*lower panel*). n = number of patients, *****P ≤ 0.00005

revealed that RRN3 is significantly overexpressed in these cancer types compared to adjacent normal tissues (Fig. 1a). Additionally, unsupervised clustering analysis of single-cell transcriptome data from LUAD, PRAD, and BRCA tumors identified a distinct subset of cells with high RRN3 expression (Fig. 1b). GSEA of these clusters demonstrated significant enrichment of genes associated with key cancer hallmarks including epithelial-mesenchymal transition (EMT), chemoresistance, and oncogenic signaling (Fig. 1c). Furthermore, higher RRN3 expression was observed in patients not responding to therapy compared to responders in LUAD, BRCA, and PRAD (Fig. 1d, box plots). ROC analysis identified RRN3 expression as a significant predictor (AUC > 0.5) of reduced therapeutic

response across these cancer types (Fig. 1d, ROC curves, lower panel). Collectively, these findings implicate RRN3 in tumor progression and therapy resistance, highlighting its potential as a prognostic biomarker and therapeutic target.

Virtual screening and molecular docking identify NSH76 as a potential RRN3 ligand

To discover small molecule ligands targeting RRN3, we performed virtual screening and docking studies utilizing the cryo-EM structure of human RRN3 (PDB ID: 7OBA). The RRN3 structure was optimized using the Schrödinger Protein Preparation Wizard, with the TAF1B, TAF1 C, and POLR1 F binding sites

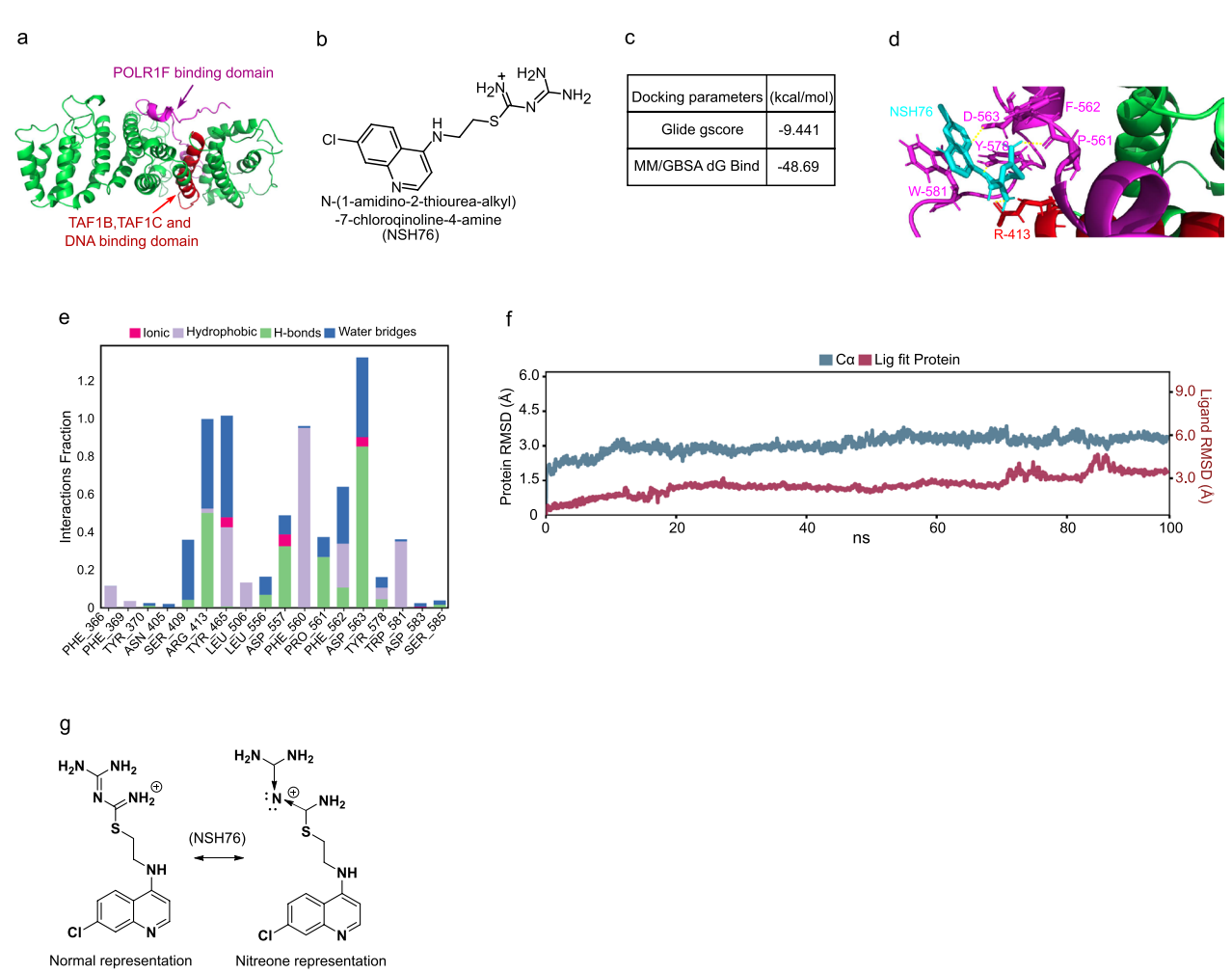


Fig. 2 Identification and characterization of NSH76 as a potential RRN3 inhibitor. a Cryo-EM structure of human RRN3 with distinct domains interacting with Pol I and SL1(PDB ID: 70BA). b Chemical structure of NSH76. c Docking analysis of RRN3 with NSH76 showing the Glide score (predicted binding affinity), and the MM/GBSA ΔG bind score (estimate of the binding free energy). d Molecular docking pose of NSH76 within the RRN3 binding pocket, highlighting interactions with critical amino acids. e Histogram illustrating the predicted contribution of amino acid residues to hydrogen bonding and hydrophobic interactions with NSH76. f Root Mean Square Deviation plot depicting the temporal stability of the RRN3-NSH76 complex during the simulation. g Electronic structure analysis showing 2D structure of NSH76 in both normal and nitreonic forms

designated as the target binding pocket for docking simulations with our in-house compound libraries (Fig. 2a). Approximately 30 synthesized compounds from our in-house library were docked to assess their potential to interact with RRN3. Molecular docking identified NSH76 as the most potential RRN3-targeting ligand, with a Glide gscore of -9.441. MM/GBSA binding free energy calculations further confirmed a strong and stable interaction between NSH76 and RRN3, yielding a ΔG _bind value of -48.69 kcal/mol (Fig. 2b, c). Interaction analysis revealed that NSH76 engages key residues R-413, P-561, F-562, D-563, Y-578, and W-581, essential for RRN3 interactions with TAF1B/ TAF1 C and POLR1 F (Fig. 2d). A binding interaction histogram highlighted the critical roles of these amino acids in hydrogen bonding and hydrophobic interactions with NSH76 (Fig. 2e). Molecular dynamics simulations further validated the stability of the RRN3-NSH76 complex, with the RMSD trajectory exhibiting minimal fluctuations throughout the simulation, indicating a stable binding conformation (Fig. 2f). To characterize the 2D structure and electronic properties of NSH76, quantum chemical analyses were performed using Density Functional Theory (DFT) with Gaussian16 software. Geometry optimization and frequency calculations at the B3LYP/6-311+G(d,p) level revealed nitreone characteristics in NSH76 (Fig. 2g, Additional File 1). These findings suggest that NSH76 is a promising RRN3-targeting small molecule with stable binding and favorable energetic properties.

NSH76 specifically binds to RRN3

The synthesis of NSH76 was achieved through a fourstep process, obtaining a final product with 82% yield (Fig. 3a, details in materials and methods). Next, to investigate the binding interaction between NSH76 and RRN3, we employed two complementary biochemical assays: DARTS and CD spectroscopy. DARTS analysis revealed that NSH76 dose-dependently protectsRRN3 against Pronase-mediated proteolysis (Fig. 3b), indicating a direct binding interaction that preventsRRN3 from degradation. To further investigate the specific NSH76-RRN3 interactions, we purified the RRN3 protein. Immunoblot analysis verified the purity and homogeneity of the isolated protein (Fig. 3c). Subsequent CD spectroscopy analysis revealed significant alterations in the secondary structure of RRN3 upon NSH76 binding. The addition of NSH76 induced a dose-dependent shift in the CD spectrum, characterized by changes in ellipticity at specific wavelengths, indicating conformational rearrangement in RRN3 upon ligand interaction (Fig. 3d). These findings indicate a direct interaction between the NSH76 and RRN3, validating NSH76 as a potential RRN3 inhibitor.

NSH76 selectively inhibits Pol I transcription in cancer cells

To determine whether cancer cells exhibit a higher dependence on RRN3 for rRNA synthesis, we analyzed RRN3 expression levels and measured 47S pre-rRNA synthesis in both cancerous and non-cancerous cells. Expression analysis revealed that cancer cell lines (A549, PC3, and MCF7) exhibited significantly higher RRN3

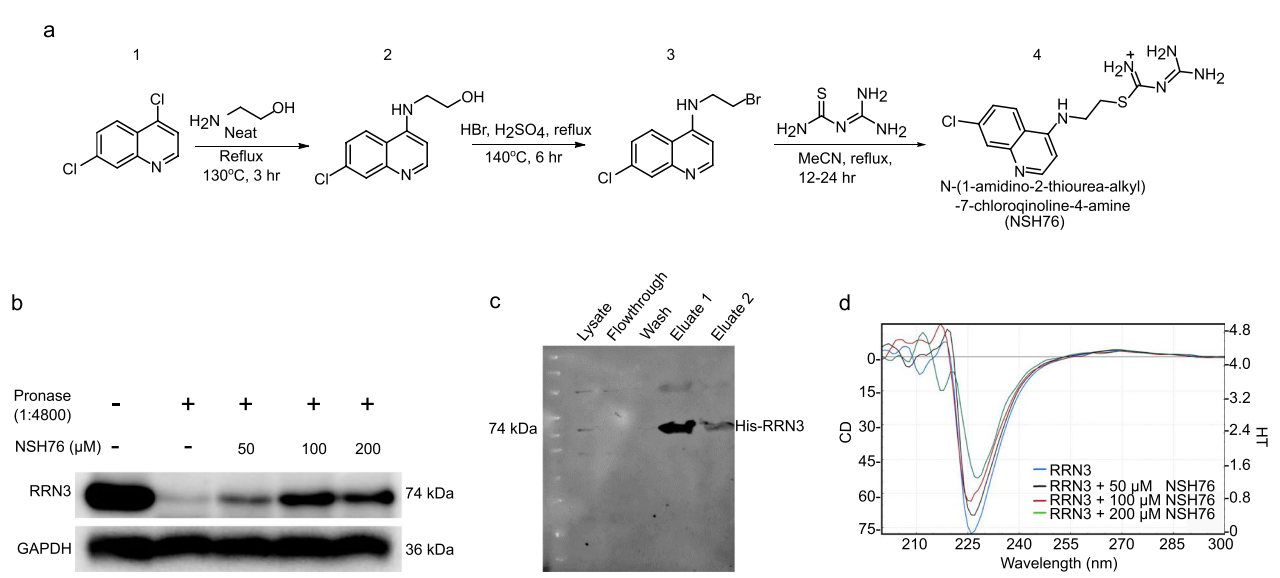


Fig. 3 NSH76 chemistry. a Scheme outlining the synthesis of NSH76. b Immunoblot showing dose-dependent protection of RRN3 against Pronase-mediated proteolysis by NSH76. c Immunoblot showing the purified RRN3 protein purity and homogeneity. d Circular dichroism spectral analysis showing the spectra of RRN3 alone and the dose-dependent spectral changes of RRN3 in the presence of NSH76. All experiments were performed in at least three biological replicates

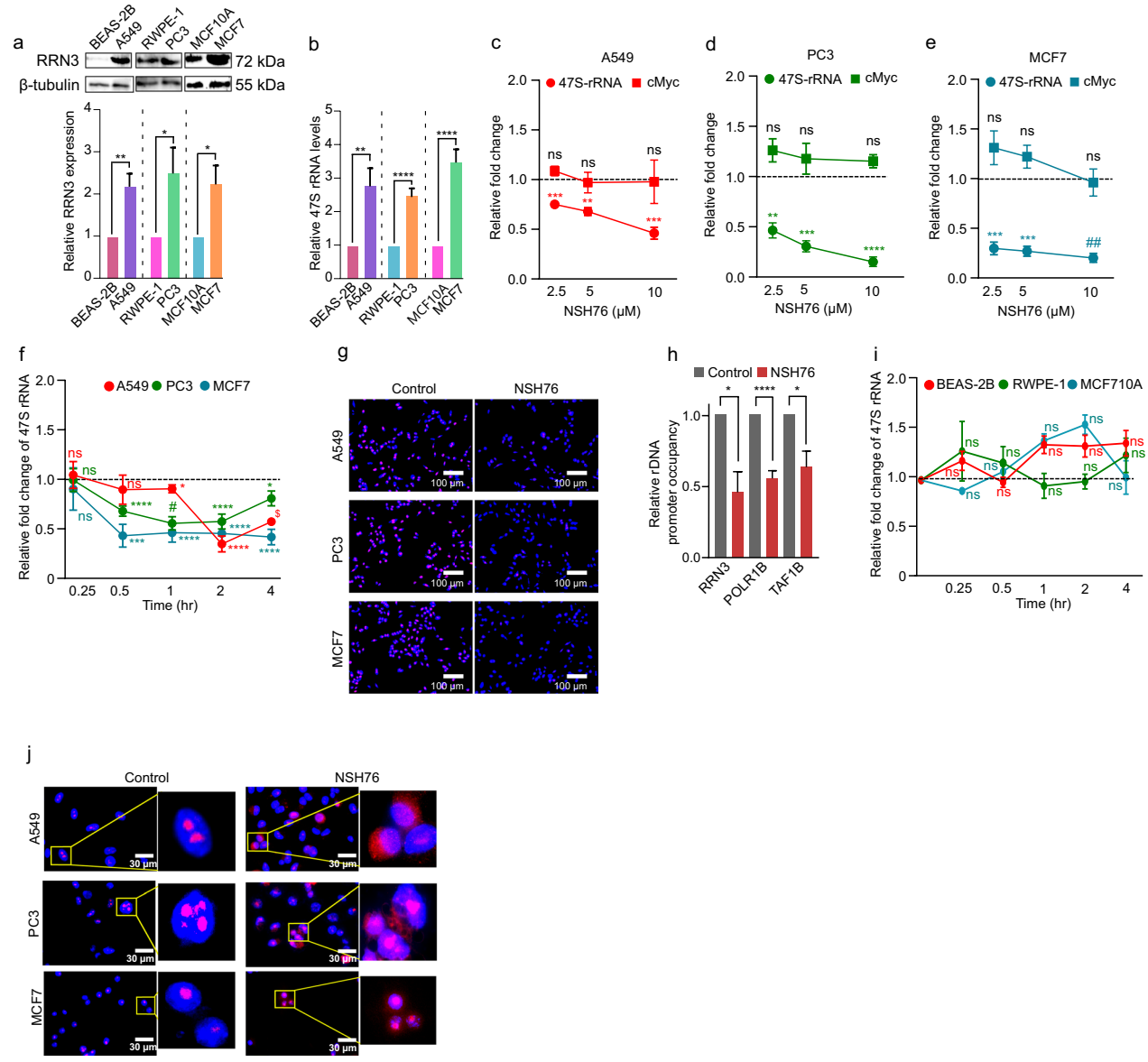


Fig. 4 NSH76 selectively inhibits Pol I transcription. Representative immunoblots showing relative RRN3 protein levels (**a**, *upper panel*) and bar graphs showing relative mRNA levels of RRN3 (**a**, *lower panel*), and 47 s rRNA (**b**) in cancerous cells (A549, MCF7, and PC3) compared to non-cancerous cells (BEAS-2B, MCF10 A, and RWPE-1). Quantitative PCR (QPCR) analysis showing 47S rRNA and cMyc expression levels in A549 (**c**), PC3 (**d**), and MCF7 (**e**) cells treated with increasing concentrations of NSH76, data normalized to actin levels. **f** QPCR analysis showing time-dependent decrease in 47S rRNA levels in A549, PC3, and MCF7 cells treated with NSH76. **g** Fluorescence images depicting reduced EU incorporation in response to NSH76 treatment in A549, PC3, and MCF7 cells, indicating reduced de novo rRNA synthesis. **h** ChIP-qPCR data showing the relative promoter occupancy of RRN3, TAF1B, and POLR1B in NSH76-treated A549 cells. **i** QPCR analysis showing no significant changes in 47S rRNA levels in non-cancerousBEAS-2B, MCF10 A, and RWPE-1 cells treated with NSH76. **j** Immunofluorescence images depicting the translocation of NPM1 to the nucleus and disruption of the nucleolus in response to NSH76 treatment in A549, PC3, and MCF7 cells, DAPI staining (*blue*), NPM1 (*red*). All experiments were performed in at least three biological replicates. Error bars indicate mean ± SEM. * $P \le 0.05$, ** $P \le 0.005$, ** $P \le 0.005$, ** $P \le 0.0005$, ** $P \le 0.00$

levels at both protein (Fig. 4a, upper panel) and mRNA levels (Fig. 4a, lower panel) compared to their non-cancerous counterparts (BEAS-2B, MCF10 A, and RWPE-1). Consistently, 47S pre-rRNA synthesis was markedly elevated in RRN3-high cancer cells (Fig. 4b), indicating

that increased RRN3 expression enhances rRNA synthesis, further supporting the therapeutic relevance of targeting RRN3. Next, to evaluate the specificity of NSH76 in inhibiting Pol I transcription, we treated A549, PC3, and MCF7 cells with varying doses of NSH76 and

measured Pol I transcription, using Pol II activity as a control to assess selectivity. Pol I activity was quantified by 47S rRNA transcripts, while cMyc expression served as a surrogate marker for Pol II activity. NSH76 treatment elicited a remarkable, dose-dependent reduction in 47S rRNA levels in A549 (Fig. 4c), PC3 (Fig. 4d), and MCF7 (Fig. 4e) cells, while cMyc expression remaining unaltered. This selective inhibition of Pol I transcription was further corroborated by a time-dependent decrease in rRNA levels across all tested cell lines (Fig. 4f). Additionally, NSH76-treated cells displayed a marked reduction in EU incorporation, further confirming its ability to inhibit de novo rRNA synthesis (Fig. 4g). Given that RRN3 is essential for PIC formation at the rDNA promoter, we performed ChIP assays to assess the impact of NSH76 on the occupancy of PIC components at the rDNA promoter. ChIP-qPCR analysis revealed a significant reduction in the occupancy of RRN3, TAF1B, and POLR1B at the rDNA promoter in response to NSH76 treatment (Fig. 4h). Notably, treatment with NSH76 (10 μM) did not inhibit rRNA synthesis in non-cancerous cells (Fig. 4i). Pol I transcription inhibition is associated with nucleolar stress, characterized by the translocation of nucleophosmin (NPM1) from the nucleolus to the nucleoplasm [38]. Strikingly, immunofluorescence analysis revealed that NSH76 disrupted nucleolar morphology and caused NPM1 redistribution, underscoring NSH76 capacity to trigger nucleolar stress through selective Pol I inhibition (Fig. 4j). These findings establish NSH76 as a selective Pol I inhibitor that effectively suppresses rRNA synthesis, disrupts PIC formation, and induces nucleolar stress, in RRN3-high cancer cells.

NSH76 induces anti-proliferative effects via p53 activation, cell cycle arrest, and apoptosis

To investigate the functional consequences of NSH76-mediated Pol I inhibition, we assessed its effects on cell proliferation, cell cycle progression, and apoptosis in

both cancerous and non-cancerous cell lines. NSH76 treatment selectively inhibited cell proliferation in cancer cells, yielding IC-50 values of 7.52, 3.73, and 4.04 µM in A549, PC3, and MCF7 cell lines, respectively. In contrast, non-cancerous cells exhibited significantly higher IC-50 values of 48.41, 57.68, and 61.74 μM in BEAS-2B, RWPE-1, and MCF10 A cells, respectively (Fig. 5a). Notably, NSH76 treatment induced a significant, dose-dependent reduction in cell viability in cancer cell lines (Fig. 5b), while exerting only marginal effects on non-cancerous cells, even at higher concentrations (Fig. 5c). CFSE staining analysis further revealed that NSH76 treatment (at IC-50) significantly reduced cell proliferation in cancer cell lines compared to untreated controls (Fig. 5d and Additional Fig. S1a). Additionally, NSH76 treatment significantly impaired colony formation in A549, PC3, and MCF7 cells (Fig. 5e). Thus, NSH76 selectively inhibits cancer cell proliferation and clonogenicity while sparing non-cancerous cells.

Pol I transcription inhibition triggers nucleolar stress, stabilizing p53 and inducing cell cycle arrest and apoptosis [38]. In line with this, NSH76 treatment significantly elevated p53 levels in wild-type p53 cell lines A549, LNCaP, and MCF7 (Fig. 5f). Furthermore, qPCR analysis revealed that this increase in p53 was associated with the transcriptional activation of its downstream target, p21, a key regulator of the G1/S checkpoint (Fig. 5g). Following this, we examined the influence of NSH76 on cell cycle dynamics. NSH76 treatment led to a marked decrease in S-phase cells and an increase in G1-phase cells, indicating G1-phase arrest (Fig. 5h and Additional Fig. S1b). Next, to assessed the apoptotic effects of NSH76 in both cancer and non-cancerous cell lines with NSH76 (at IC-50). Flow cytometry analysis revealed a significant increase in apoptosis in cancer cells treated with NSH76 compared to non-cancerous cells (Fig. 5i and Additional Fig. S1c and d). This apoptotic response was associated with an upregulation of pro-apoptotic markers BAK,

(See figure on next page.)

Fig. 5 Effects of NSH76 on cell fate. **a** IC-50 values showing differential sensitivity of cancer and non-cancerous cells to NSH76. **b** Dose-dependent effect of NSH76 on the viability of cancer cells and **c** non-cancerous cells. **d** Histograms illustrate CFSE-labeled flow cytometry analysis depicting the percentage of proliferating cells in NSH76-treated cells (at IC-50), bar graphs represent the quantification of proliferating cells. **e** Images showing clonogenicity of NSH76-treated A549, PC3 and MCF7 cells compared to respective controls, bar graph showing relative colony counts. **f** Immunoblot represents increased p53 expression in NSH76-treated cells, bar graph showing quantification of relative band intensity. **g** QPCR analysis showing reduced p21 expression in NSH76-treated cells compared to controls. **h** Flow cytometry analysis showing cell cycle distribution in NSH76-treated cells compared to controls. **i** Bar graph showing the percentage of apoptosis in NSH76-treated cancerous (A549, PC3 and MCF7) and non-cancerous cells (BEAS-2B, RWPE-1 and MCF10 A), as determined by flow cytometry. **j** QPCR analysis showing altered apoptotic markers expression in NSH76-treated cancer cells in comparison to control. **k** Reduced EU incorporation in tumor spheroids in response to NSH76. **I** Immunofluorescence images showing decreased Ki67 expression in tumor spheroids treated with NSH76. **m** DIC and fluorescence images showing increased apoptosis in a time-dependent manner in tumor spheroids treated with NSH76, line graphs indicate relative spheroid size. All experiments were performed in at least three biological replicates. Error bars indicate mean \pm SEM. * $P \le 0.005$, *** $P \le 0.0005$, **** $P \le 0.$

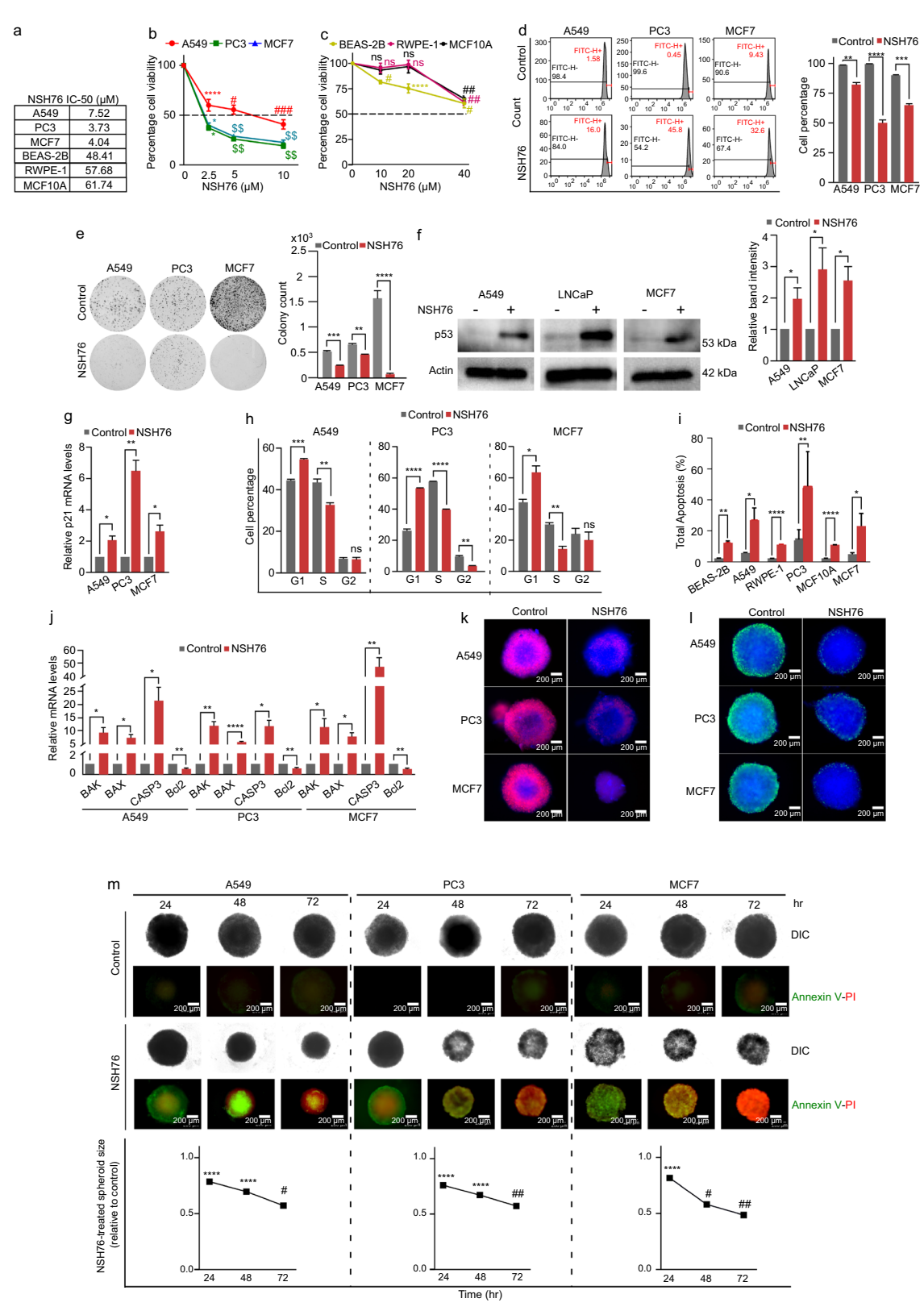


Fig. 5 (See legend on previous page.)

BAX, and CASP3, with a concurrent downregulation of the anti-apoptotic protein Bcl2 in NSH76-treated cancer cells (Fig. 5j). Tumor spheroids closely resemble in vivo solid tumors and widely utilized for screening anticancer drugs. Notably, NSH76 treatment in tumor spheroids resulted in significantly suppressed de novo rRNA synthesis, as evidenced by reduced EU incorporation (Fig. 5k). Immunofluorescence staining further revealed a substantial decrease in the expression of proliferation marker Ki67 expression, suggesting that NSH76 effectively reduced cell proliferation within the tumor spheroids (Fig. 51). Additionally, Annexin V/PI fluorescence imaging demonstrated a time-dependent increase in apoptotic cells, marked by the appearance of a necrotic core and a significant reduction in spheroid size (Fig. 5m). These findings strongly indicate that NSH76 inhibits proliferation by activating p53-p21, inducing cell cycle arrest, and modulating apoptotic gene expression, leading to apoptosis.

NSH76 enhances chemosensitivity in drug-resistant cells

Elevated Pol I transcription has been implicated in chemoresistance [16]. To assess whether NSH76-mediated Pol I inhibition affects drug resistance, we generated cisplatin- and doxorubicin-resistant A549 cell lines (A549-Cis^R and A549-Dox^R). These resistant cells displayed significantly higher IC-50 values for cisplatin (16.68 vs. 7.11 µM) and doxorubicin (1.66 vs. 0.44 µM) compared to their parental cell line (Fig. 6a). Notably, A549-Cis^R and A549-Dox^Rcells demonstrated significantly higher viability following cisplatin and doxorubicin treatment, respectively, compared to their parental cells (Fig. 6b, c). In addition, flow-cytometric analysis revealed a reduced apoptosis inA549-Cis^R and A549-Dox^Rcells in response to cisplatin and doxorubicin (Fig. 6d, e, and Additional Fig. S2a and S2b). Collectively, these results validate the successful development of cisplatin- and doxorubicinresistant A549 cell lines. Next, we evaluated the expression of RRN3 and rRNA synthesis in A549-Cis^R and A549-Dox^R cells. qPCR analysis revealed a significant upregulation of RRN3 (Fig. 6f) and increased rRNA levels (Fig. 6g, h) in these resistant cells, suggesting that elevated RRN3 expression and enhanced Pol I transcription may contribute to the drug-resistant phenotype. Subsequently, we evaluated the anti-proliferative effects of NSH76 on A549-Cis^R and A549-Dox^Rcells. Notably, NSH76 treatment significantly inhibited cell proliferation in both resistant cell lines, with IC-50 values of 2.85 and 2.63 µM, respectively, which were substantially lower than the IC-50 value observed in parental A549 cells (7.38 μM) (Fig. 6i). Furthermore, NSH76 treatment resulted in a dose-dependent reduction in cell viability in A549-Cis^R and A549-Dox^Rcells compared to parental cells (Fig. 6j). Additionally, NSH76 treatment induced a marked increase in apoptosis in A549-Cis^R and A549-Dox^R cells, compared to parental A549 cells (Fig. 6k and Additional Fig. S2c). To further evaluate the anti-tumor potential of NSH76 beyond its cytotoxic and chemosensitizing effects, we assessed its impact on cancer cell migration and invasion. Notably, In vitro invasion and migration assays demonstrated a remarkable reduction in migratory and invasive capacities of A549, PC3 and MCF7 cells upon NSH76 treatment (Fig. 6l, m). In summary, these findings demonstrate the potential of NSH76-mediated inhibition of RRN3 and Pol I transcription in sensitizing Cisplatin and Doxorubicin resistant cells, but also suppresses the migratory and invasive potential of cancer cells migratory and invasive potential.

NSH76 exhibits non-genotoxic and non-mutagenic properties

To assess the safety profile, we evaluated the potential genotoxicity of NSH76. Our results showed that, unlike doxorubicin, NSH76 treatment did not induce DNA damage, as evidenced by the absence of comet tails in the alkaline comet assay (Fig. 7a) and the lack of yH2 AX foci in immunofluorescence analysis (Fig. 7b). Additionally, the mutagenic potential of NSH76 was evaluated using the V79 cell mutagenicity assay, which revealed no mutant colonies following NSH76 treatment, in contrast to significant mutagenesis observed in benzopyrene (known mutagen) treated cells (Fig. 7c). Consistently, the micronucleus assay showed no chromosomal damage following NSH76 treatment, as indicated by the absence of micronucleus formation (Fig. 7d). Collectively, these results demonstrate that NSH76 possesses non-genotoxic and non-mutagenic properties.

Discussion

Aberrant Pol I transcription fuels sustained ribosome biogenesis, supporting uncontrolled cancer cell proliferation and oncogenesis. Targeting Pol I transcription has emerged as a promising cancer therapy strategy [13]. We investigated the therapeutic potential of NSH76, a small molecule inhibitor targeting Pol I-specific transcription factor RRN3. NSH76 selectively inhibits Pol I transcription at the initiation step, exhibiting potent antiproliferative and cytotoxic effects in cancer cells and tumor spheroids, and exhibits minimal toxicity towards noncancerous cells. Notably, NSH76 overcomes resistance in cancer cells, reversing the resistant phenotype. Importantly, NSH76-induced Pol I transcription inhibition does not induce DNA damage or mutagenesis, highlighting its favorable safety profile. These findings demonstrate NSH76 therapeutic efficacy and support its further development as a lead molecule for cancer therapy.

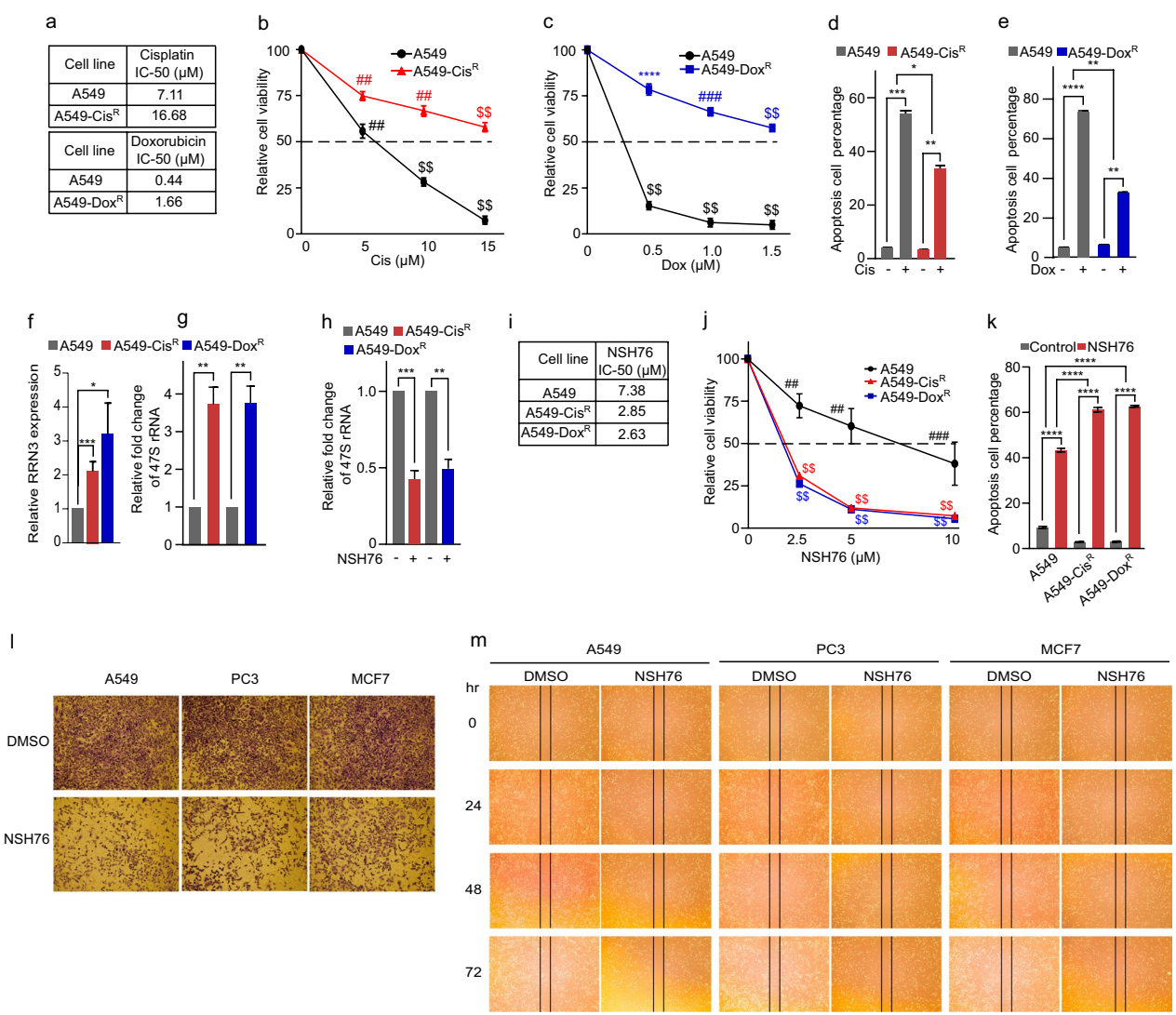


Fig. 6 NSH76 enhances cisplatin and doxorubicin sensitivity in resistant cells. **a** Cisplatin and doxorubicin IC-50 values are higher in the resistant cell lines (A549-Cis^R and A549-Dox^R) compared to the parental A549 cells. Line graph showing relatively higher cell viability in **b** A549-Cis^R cells (**c**) and A549-Dox^R cells in response to cisplatin and doxorubicin, respectively. Flow cytometry bar graphs represent reduced apoptosis in **d** A549-Cis^R and **e** A549-Dox^R cells treated with cisplatin or doxorubicin, respectively, compared to the controls. Bar graphs showing the relative expression of **f** RRN3 and **g** 47 s rRNA levels in A549-Cis^R and A549-Dox^R compared to parental cells. **h** Bar graph showing the reduced 47 s rRNA expression in A549-Cis^R and A549-Dox^R in response to NSH76 compared to control. **i** A549-Cis^R and A549-Dox^R cells showing lower IC-50 values for NSH76 compared to parental cells. **j** Decreased cell viability in A549-Cis^R and A549-Dox^R cells treated with increasing concentrations of NSH76. **k** Flow-cytometric analysis showing increased apoptosis in A549-Cis^R and A549-Dox^R cells treated with NSH76 in comparison with parental A549 cells. **l** Matrigel invasion assay indicating reduced invasion of A549, PC3, and MCF7 cells treated with IC₅₀ concentrations of NSH76 compared to untreated controls. **m** Scratch wound healing assay showing reduced migration of A549, PC3, and MCF7 cells treated with IC₅₀ concentrations of NSH76 compared to untreated controls. All experiments were performed in at least three biological replicates. Error bars indicate mean ± SEM. *P ≤ 0.005, **P ≤ 0.005, **P ≤ 0.005, **P ≤ 0.0005, **P ≤

Nitreones are cationic species, characterized by a positively charged nitrogen center with two coordination bonds and two lone pairs of electrons [39–43]. In its neutral form, NSH76 is highly basic and readily undergoes protonation under physiological conditions due to its exceptionally high proton affinity (236.65)

kcal/mol). This protonation efficiently converts NSH76 into its active, cationic nitreone state. Notably, this unique architecture is shared by various established drugs including, Metformin, Proguanil, Chlorhexidine, which exhibit nitreone character in their cationic states, contributing to their therapeutic efficacy. Therefore, the

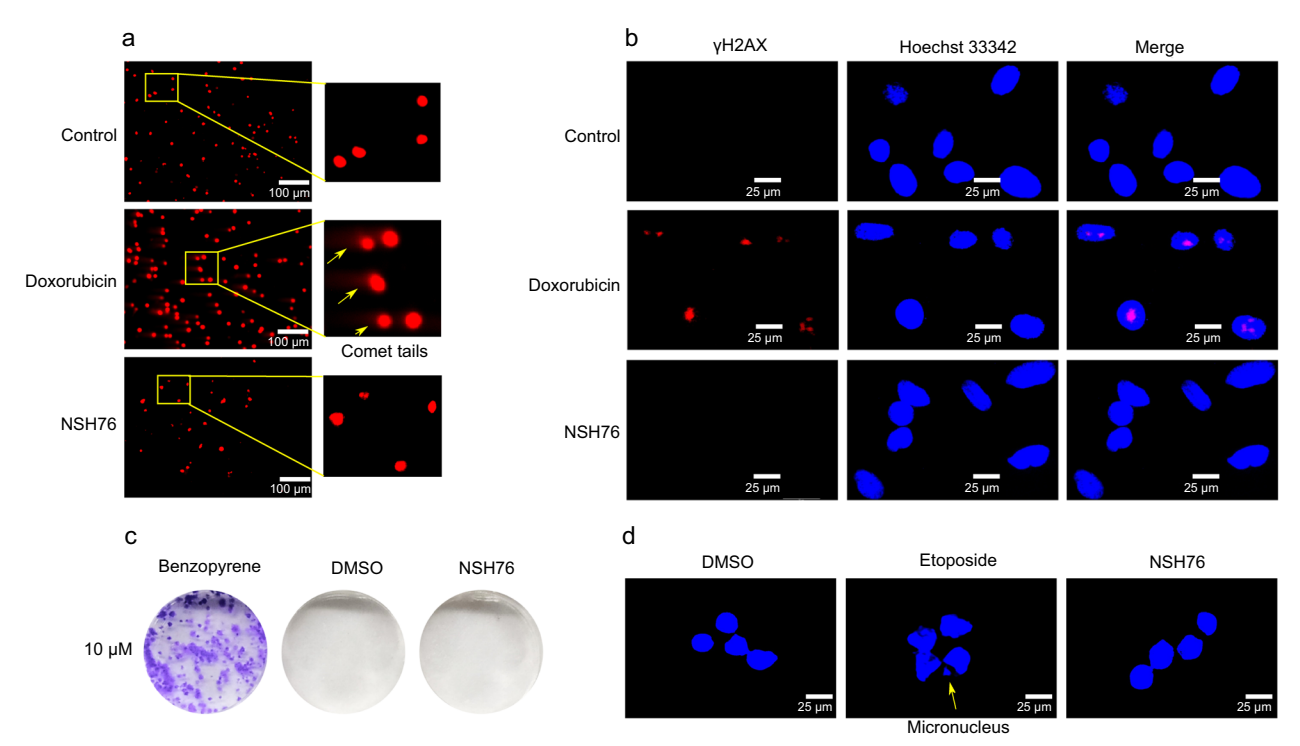


Fig. 7 Effects of NSH76 on genomic integrity. **a** Representative images showing comet tails in response to NSH76 (10 μM) or doxorubicin (1 μM) treatment in A549 cells. **b** Immunofluorescence images showing γH2 AX expression in NSH76 (10 μM) or doxorubicin-treated (1 μM) in A549 cells. **c** Images showing mutagenic clone formation in V79 cells treated with NSH76 in comparison to benzopyrene treatment. **d** Representative images showing micronucleus formation in A549 cells treated with NSH76 (10 μM) or etoposide (1 μM). All experiments were performed in at least three biological replicates

nitreone architecture of NSH76 could be attributed to its biological activity.

Despite the initial success of CX-5461, the first-inclass Pol I inhibitor, recent investigations have elucidated that its primary target is TOP2B, with secondary effects on Pol I transcription [23]. Similarly, BMH-21 induces POLR2 A degradation, the largest subunit of RNA Pol II transcription machinery, and interferes with the TOP-2Bactivity, contributing to the cytotoxicity [25]. These off-target activities may contribute to the unintended cytotoxic effects, limiting the therapeutic potential of these compounds. Unlike CX5461, which disrupts rDNA topology, and BMH-21, which triggers Pol I degradation, targeting the Pol I-specific PIC enhances specificity and reduces toxicity. This approach exploits the unique essentiality and distinct expression of PIC components in tumors compared to non-tumor tissues.

RRN3 plays a pivotal role in regulating Pol I transcription initiation by recruiting the Pol I enzyme complex to the rDNA promoter, directed by SL1 [9]. Notably, RRN3 also serves as a convergence point for oncogenic signals from cMyc, and mTOR pathways, making it a critical node in breast cancer metabolism [44]. Genetic inhibition of RRN3 has demonstrated potent anti-tumor effects

in breast [15], lung [16] and pancreatic [14] cancer models, resulting in Pol I transcription inhibition and reduced tumor burden. This is consistent with previous findings that selective inhibition of rDNA transcription by targeting the Pol I-RRN3 interface by small-peptide effectively suppresses tumor growth [45]. Our study reinforces RRN3 potential as a therapeutic target, as pharmacological inhibition with NSH76 specifically disrupts PIC occupancy at the rDNA promoter, leading to Pol I transcription inhibition. These findings underscore RRN3 critical role in cancer cell proliferation and position it as a promising target for cancer therapy.

Stringent regulation of Pol I transcription is crucial for maintaining nucleolar integrity and cellular homeostasis, and its disruption leads to structural reorganization of the nucleolus, a hallmark of cancer [46], and activates nucleolar stress pathway (NSP). Cancer cells exhibit higher Pol I transcription than non-cancerous differentiated cells, making them more susceptible to Pol I transcription inhibition-induced nucleolar stress, providing a broad therapeutic window for targeting cancer cells. Consistent with this, NSH76, showed broad-spectrum antiproliferative activity in cancer cells while having a minimal effect on normal cells. The

upregulated Pol I transcription in cancer cells underlies the high sensitivity of NSH76, highlighting its potential as a selective anticancer therapeutic. Furthermore, Pol I inhibition leads to the activation of nucleolar stress and the NSP to trigger downstream effects, including cell cycle arrest and apoptosis [19]. One of the critical hallmarks of Pol I inhibition-mediated NSP is p53 activation. Following nucleolar stress, ribosomal proteins RPL5 and RPL11 bind to MDM2 and disrupt p53-MDM2 interaction, leading to the p53 activation. The activated p53 induces apoptosis via transcriptional activation of target genes, including p21 and pro-apoptotic marker BAX [47]. Consistent with the above studies, we found that NSH76 activates p53 in p53 wild-type cells. The NSH76-mediated Pol I inhibition and subsequent activation of the nucleolar stress could be responsible for p53 activation, and concomitant activation of its target genes led to the activation of the intrinsic apoptosis pathway in cancer cells.

Chemoresistance is a major limiting factor for successful chemotherapy. Recent studies have implicated hyperactive Pol I transcription in the development of therapeutic resistance. Notably, taxane-resistant ovarian cancer cells exhibit upregulated Pol I transcription [5]. Moreover, our recent work has shown that miRNAmediated inhibition of basal Pol I transcription machinery components enhances cisplatin sensitivity in LUAD cells [16]. Consistent with these findings, our work reveals that potent inhibition of Pol I transcription by NSH76 sensitizes resistant cells to cisplatin and doxorubicin. Chemoresistant cells frequently exhibit upregulated Pol I transcription, conferring a survival advantage. This heightened Pol I activity presents a vulnerable target for NSH76 inhibition sensitizing resistant cells to chemotherapeutics. Moreover, we demonstrated that NSH76 activates p53, which in turn triggers the intrinsic apoptotic pathway. Since chemotherapeutic agents rely on functional p53 to induce cancer cell death, NSH76mediated p53 activation and subsequent apoptosis may represent a key mechanism for enhancing drug sensitivity. Additionally, we observed that NSH76 treatment significantly reduced the migratory and invasive capacities of A549, PC3, and MCF7 cells. Pol I transcription plays a critical role in sustaining EMT processes, a key driver of metastasis [48]. By inhibiting Pol I, NSH76 disrupts rRNA synthesis, inducing nucleolar stress and activating tumor suppressors like p53. This activation subsequently modulates EMT-related processes, including reduced cellular motility and invasion. Therefore, NSH76 not only sensitizes cancer cells to chemotherapy but also limits their invasiveness and migratory potential, making it a promising therapeutic strategy to overcome both chemoresistance and tumor progression.

Chemotherapy-induced DNA damage presents a significant challenge in cancer chemotherapy, reducing treatment efficacy and causing adverse effects like mutations and genome instability [49]. Notably, CX-5461 induces significant DNA damage, as evidenced by the rapid induction of yH2 AX within 3 h of treatment [50]. Moreover, a recent study demonstrated that CX-5461 causes irreversible mutagenesis, surpassing the mutagenic effects of the known mutagen benzopyrene, thus severely limiting its clinical utility [51]. Moreover, CX-5461-mediated inhibition of TOP2B activity could be responsible for DNA damage and subsequent mutations. In contrast, we have shown that NSH76 do not induce cellular DNA damage, or mutagenesis, highlighting differences in the biological effects of NSH76. Thus, NSH76 may offer a safer alternative for therapeutic inhibition of Pol I transcription inhibition.

Conclusion

Our study demonstrates the therapeutic potential of NSH76 in cancer therapy through selective Pol I transcription inhibition and lays the groundwork for preclinical and clinical studies, providing a critical stepping stone for the development of NSH76 as a novel therapeutic agent for neoplastic diseases.

Abbreviations

RNA polymerase I
Ribosomal RNA
Ribosomal DNA
Pre-initiation complex
Selectivity factor 1
Upstream binding factor
TATA-binding protein
TBP-associated factors
Topoisomerase IIβ
Lung adenocarcinoma

NSH76 N-(1-amidino-2-thiourea-alkyl-7-chloroquinoline-4-amine)

ROC Receiver operating characteristic MD Molecular dynamics

RMSD Root mean square deviation
DCM Dichloromethane
ACN Acetonitrile

ACN Acetonitrile
IC-50 Inhibitory Concentration
A549-CisR Cisplatin-resistant A549 cell line
Doxorubicin-resistant A549 cell line

DMSO Dimethyl Sulfoxide

IPTG Isopropyl β-D-1-thiogalactopyranoside

SDS-PAGE Sodium dodecyl sulfate–polyacrylamide gel electrophoresis

DARTS Drug affinity responsive target stability

PBS Phosphate-buffered saline
PVDF Polyvinylidene difluoride
ECL Enhanced chemiluminescence

CD Circular dichroism
qPCR Real-time quantitative PCR
EU 5-Ethynyl-2'-uridine
BSA Bovine serum albumin

DPX Dibutyl phthalate polystyrene xylene

RT Room temperature

DPBS Dulbecco's phosphate-buffered saline

PI Propidium iodide
SEM Standard error of the

SEM Standard error of the mean

ANOVA Analysis of variance PRAD Prostate adenocarcinoma

BRCA Breast cancer

TCGA The Cancer Genome Atlas
GSEA Gene set enrichment analysis
EMT Epithelial mesenchymal transition
DFT Density functional theory

NPM1 Nucleophosmin
NSP Nucleolar stress pathway

Supplementary Information

The online version contains supplementary material available at https://doi.org/10.1186/s12967-025-06588-y.

Additional file 1: Table 1. List of primers and antibodies used in this study. Additional file 2: Electronic structure analysis of NSH76.

Additional file 3: Fig. S1. Flow Cytometry analysis of NSH76-treated Cells. a. CFSE proliferation histograms showing reduced proliferation of cells treated with NSH76. b. Cell cycle histograms indicating G1-phase arrest in cells treated with NSH76. c. Annexin V-Pl apoptosis histograms depicting increased apoptosis in NSH76-treated non-cancerous cells. d. Annexin V-Pl apoptosis histograms depicting increased apoptosis in NSH76-treated cancer cells.

Additional file 4: Fig. S2: Flowcytometry analysis of cisplatin- and doxorubicin- resistant cells. a. Annexin V-PI apoptosis histograms of cisplatin-treated A549 and A549-Cis^R cells, showing decreased apoptosis in resistant cells. b. Annexin V-PI apoptosis histograms of doxorubicin-treated A549 and A549-Dox^R cells, showing decreased apoptosis in resistant cells. c. Annexin V-PI apoptosis histograms of NSH76-treated A549, A549-Cis^R, and A549-Dox^R cells, demonstrating increased apoptosis in resistant cells.

Acknowledgements

Thanks to Mehak Sood, NIPER Mohali, for her assistance in NSH76 synthesis, and Deepika Antil for proof reading the manuscript.

Author contributions

SSS, MS, AK, performed experiments, analyzed and curated the data, SS performed computational analysis, KJ performed docking and ligand screening, synthesized NSH76 supervised by PVB, SB and SA and NA expressed and purified RRN3 protein supervised by IR. SN conceived and designed the study, supervised the work, secured funding and drafted the manuscript.

Funding

This work was supported by the SERB-ECR grant awarded to SN.

Availability of data and materials

The data generated in the study is available in the manuscript and its supplementary data files.

Declarations

Ethics approval and consent to participate

Not applicable.

Consent for publication

All authors agreed to this publication.

Competing interests

The authors declare no competing interests.

Author details

¹Department of Biomedical Engineering, Indian Institute of Technology Ropar, Rupnagar, Punjab 14000, India. ²Department of Medicinal Chemistry, National Institute of Pharmaceutical Education and Research (NIPER), S.A.S. Nagar, Punjab 160062, India. ³Department of Biotechnology, National Institute of Pharmaceutical Education and Research (NIPER), S.A.S. Nagar, Punjab 160062, India.

Received: 4 March 2025 Accepted: 7 May 2025 Published online: 20 October 2025

References

- Moreno-Morcillo M, Taylor NM, Gruene T, Legrand P, Rashid UJ, Ruiz FM, et al. Solving the RNA polymerase I structural puzzle. Acta Crystallogr D Biol Crystallogr. 2014;70(Pt 10):2570–82.
- Goodfellow SJ, Zomerdijk JC. Basic mechanisms in RNA polymerase I transcription of the ribosomal RNA genes. Subcell Biochem. 2013;61:211–36.
- Liebhaber SA, Wolf S, Schlessinger D. Differences in rRNA metabolism of primary and SV40-transformed human fibroblasts. Cell. 1978;13(1):121–7.
- Bywater MJ, Pearson RB, McArthur GA, Hannan RD. Dysregulation of the basal RNA polymerase transcription apparatus in cancer. Nat Rev Cancer. 2013;13(5):299–314.
- Cornelison R, Dobbin ZC, Katre AA, Jeong DH, Zhang Y, Chen D, et al. Targeting RNA-polymerase I in both chemosensitive and chemoresistant populations in epithelial ovarian cancer. Clin Cancer Res. 2017;23(21):6529–40.
- Elhamarnsy AR, Metge BJ, Alsheikh HA, Shevde LA, Samant RS. Ribosome biogenesis: a central player in cancer metastasis and therapeutic resistance. Cancer Res. 2022;82(13):2344–53.
- Grummt I. Wisely chosen paths–regulation of rRNA synthesis: delivered on 30 June 2010 at the 35th FEBS Congress in Gothenburg. Sweden FEBS J. 2010;277(22):4626–39.
- Pelletier J, Thomas G, Volarevic S. Ribosome biogenesis in cancer: new players and therapeutic avenues. Nat Rev Cancer. 2018;18(1):51–63.
- Pitts S, Laiho M. Regulation of RNA polymerase I stability and function. Cancers (Basel). 2022;14(23):5776.
- Ueda M, Iguchi T, Nambara S, Saito T, Komatsu H, Sakimura S, et al. Overexpression of transcription termination factor 1 is associated with a poor prognosis in patients with colorectal cancer. Ann Surg Oncol. 2015;22(Suppl 3):S1490–8.
- 11. Dai Z, Zhu W, Hou Y, Zhang X, Ren X, Lei K, et al. METTL5-mediated 18S rRNA m(6)A modification promotes oncogenic mRNA translation and intrahepatic cholangiocarcinoma progression. Mol Ther. 2023;31(11):3225–42.
- Zomerdijk JC, Beckmann H, Comai L, Tjian R. Assembly of transcriptionally active RNA polymerase I initiation factor SL1 from recombinant subunits. Science. 1994;266(5193):2015–8.
- Drygin D, Rice WG, Grummt I. The RNA polymerase I transcription machinery: an emerging target for the treatment of cancer. Annu Rev Pharmacol Toxicol. 2010;50:131–56.
- Batbayar C, Ishii N, Harimoto N, Yokobori T, Saito H, Gantumur D, et al. High RRN3 expression is associated with malignant characteristics and poor prognosis in pancreatic cancer. Int J Clin Oncol. 2023;28(7):901–12.
- Rossetti S, Wierzbicki AJ, Sacchi N. Mammary epithelial morphogenesis and early breast cancer. Evidence of involvement of basal components of the RNA polymerase I transcription machinery. Cell Cycle. 2016;15(18):2515–26.
- Saproo S, Sarkar SS, Gupta E, Chattopadhyay S, Charaya A, Kalra S, et al. MiR-330-5p and miR-1270 target essential components of RNA polymerase I transcription and exhibit a novel tumor suppressor role in lung adenocarcinoma. Cancer Gene Ther. 2023;30(2):288–301.
- 17. Yang F, Liu H, Zhao J, Ma X, Qi W. POLR1B is upregulated and promotes cell proliferation in non-small cell lung cancer. Oncol Lett. 2020;19(1):671–80.
- Zhang J, Zhang J, Liu W, Ge R, Gao T, Tian Q, et al. UBTF facilitates melanoma progression via modulating MEK1/2-ERK1/2 signalling pathways by promoting GIT1 transcription. Cancer Cell Int. 2021;21(1):543.
- Ferreira R, Schneekloth JS Jr, Panov KI, Hannan KM, Hannan RD. Targeting the RNA polymerase I transcription for cancer therapy comes of age. Cells. 2020;9(2):266.
- Drygin D, Lin A, Bliesath J, Ho CB, O'Brien SE, Proffitt C, et al. Targeting RNA polymerase I with an oral small molecule CX-5461 inhibits ribosomal RNA synthesis and solid tumor growth. Cancer Res. 2011;71(4):1418–30.
- 21. Colis L, Ernst G, Sanders S, Liu H, Sirajuddin P, Peltonen K, et al. Design, synthesis, and structure-activity relationships of

- pyridoquinazolinecarboxamides as RNA polymerase I inhibitors. J Med Chem. 2014;57(11):4950–61.
- Colis L, Peltonen K, Sirajuddin P, Liu H, Sanders S, Ernst G, et al. DNA intercalator BMH-21 inhibits RNA polymerase I independent of DNA damage response. Oncotarget. 2014;5(12):4361–9.
- Pan M, Wright WC, Chapple RH, Zubair A, Sandhu M, Batchelder JE, et al. The chemotherapeutic CX-5461 primarily targets TOP2B and exhibits selective activity in high-risk neuroblastoma. Nat Commun. 2021;12(1):6468.
- Cameron DP, Sornkom J, Alsahafi S, Drygin D, Poortinga G, Mcarthur GA, et al. CX-5461 preferentially induces Top2α-dependent DNA breaks at ribosomal DNA loci. Biomedicines. 2024;12(7):1514.
- Espinoza JA, Kanellis DC, Saproo S, Leal K, Martinez JF, Bartek J, et al. Chromatin damage generated by DNA intercalators leads to degradation of RNA Polymerase II. Nucleic Acids Res. 2024;52(8):4151–66.
- Cavanaugh AH, Hirschler-Laszkiewicz I, Hu Q, Dundr M, Smink T, Misteli T, et al. Rrn3 phosphorylation is a regulatory checkpoint for ribosome biogenesis. J Biol Chem. 2002;277(30):27423–32.
- Bhagat S, Arfeen M, Das G, Ramkumar M, Khan SI, Tekwani BL, et al. Design, synthesis and biological evaluation of 4-aminoquinolineguanylthiourea derivatives as antimalarial agents. Bioorg Chem. 2019;91: 103094.
- Tang G, Cho M, Wang X. OncoDB: an interactive online database for analysis of gene expression and viral infection in cancer. Nucleic Acids Res. 2022;50(D1):D1334–9.
- 29. Fekete JT, Gyorffy B. ROCplot.org: Validating predictive biomarkers of chemotherapy/hormonal therapy/anti-HER2 therapy using transcriptomic data of 3,104 breast cancer patients. Int J Cancer. 2019:145(11):3140–51.
- 30. Engel C, Plitzko J, Cramer P. RNA polymerase I-Rrn3 complex at 4.8 A resolution. Nat Commun. 2016;7:12129.
- Chattopadhyay S, Sarkar SS, Saproo S, Yadav S, Antil D, Das B, et al. Apoptosis-targeted gene therapy for non-small cell lung cancer using chitosan-poly-lactic-co-glycolic acid -based nano-delivery system and CASP8 and miRs 29A–B1 and 34A. Front Bioeng Biotechnol. 2023;11:1188652.
- Sarkar SS, Sharma M, Saproo S, Naidu S. LINC01116-dependent upregulation of RNA polymerase I transcription drives oncogenic phenotypes in lung adenocarcinoma. J Transl Med. 2024;22(1):904.
- Pai MY, Lomenick B, Hwang H, Schiestl R, McBride W, Loo JA, et al. Drug affinity responsive target stability (DARTS) for small-molecule target identification. Methods Mol Biol. 2015;1263:287–98.
- 34. Pfaffl MW. A new mathematical model for relative quantification in real-time RT-PCR. Nucleic Acids Res. 2001;29(9): e45.
- Lu Y, Liu Y, Yang C. Evaluating in vitro DNA damage using comet assay. J Vis Exp. 2017:128:56450.
- Bradley MO, Bhuyan B, Francis MC, Langenbach R, Peterson A, Huberman E. Mutagenesis by chemical agents in V79 chinese hamster cells: a review and analysis of the literature. A report of the Gene-Tox Program. Mutat Res. 1981;87(2):81–142.
- Uemura M, Zheng Q, Koh CM, Nelson WG, Yegnasubramanian S, De Marzo AM. Overexpression of ribosomal RNA in prostate cancer is common but not linked to rDNA promoter hypomethylation. Oncogene. 2012;31(10):1254–63.
- Liao H, Gaur A, Mauvais C, Denicourt C. p53 induces a survival transcriptional response after nucleolar stress. Mol Biol Cell. 2021;32(20):ar3.
- Patel N, Sood R, Bharatam PV. NL(2)(+) systems as new-generation phasetransfer catalysts. Chem Rev. 2018;118(18):8770–85.
- Patel N, Arfeen M, Sood R, Khullar S, Chakraborti AK, Mandal SK, et al. Can remote N-heterocyclic carbenes coordinate with main group elements? Synthesis, structure, and quantum chemical analysis of N(+) -centered complexes. Chemistry. 2018;24(24):6418–25.
- Bharatam PV, Arfeen M, Patel N, Jain P, Bhatia S, Chakraborti AK, et al. Design, synthesis, and structural analysis of divalent N(I) compounds and identification of a new electron-donating ligand. Chemistry. 2016;22(3):1088–96.
- Dubey G, Singh T, Bharatam PV. The importance of four-membered NHCs in stabilizing Breslow intermediates on benzoin condensation pathway. J Comput Chem. 2023;44(3):346–54.

- 43. Bhatia S, Bagul C, Kasetti Y, Patel DS, Bharatam PV. Divalent N(l) character in 2-(thiazol-2-yl)guanidine: an electronic structure analysis. J Phys Chem A. 2012;116(36):9071–9.
- 44. Harold CM, Buhagiar AF, Cheng Y, Baserga SJ. Ribosomal RNA transcription regulation in breast cancer. Genes (Basel). 2021;12(4):502.
- Rothblum K, Hu Q, Penrod Y, Rothblum LI. Selective inhibition of rDNA transcription by a small-molecule peptide that targets the interface between RNA polymerase I and Rrn3. Mol Cancer Res. 2014;12(11):1586–96.
- 46. Dash S, Lamb MC, Lange JJ, McKinney MC, Tsuchiya D, Guo F, et al. rRNA transcription is integral to phase separation and maintenance of nucleolar structure. PLoS Genet. 2023;19(8): e1010854.
- 47. Wang H, Guo M, Wei H, Chen Y. Targeting p53 pathways: mechanisms, structures, and advances in therapy. Signal Transduct Target Ther. 2023:8(1):92.
- Prakash V, Carson BB, Feenstra JM, Dass RA, Sekyrova P, Hoshino A, et al. Ribosome biogenesis during cell cycle arrest fuels EMT in development and disease. Nat Commun. 2019;10(1):2110.
- Jurkovicova D, Neophytou CM, Gasparovic AC, Goncalves AC. DNA damage response in cancer therapy and resistance: challenges and opportunities. Int J Mol Sci. 2022;23(23):14672.
- 50. Sanij E, Hannan KM, Xuan J, Yan S, Ahern JE, Trigos AS, et al. CX-5461 activates the DNA damage response and demonstrates therapeutic efficacy in high-grade serous ovarian cancer. Nat Commun. 2020;11(1):2641.
- Koh GCC, Boushaki S, Zhao SJ, Pregnall AM, Sadiyah F, Badja C, et al. The chemotherapeutic drug CX-5461 is a potent mutagen in cultured human cells. Nat Genet. 2024;56(1):23–6.

Publisher's Note

Springer Nature remains neutral with regard to jurisdictional claims in published maps and institutional affiliations.